



**HAL**  
open science

## Broadband high-contrast-grating-type waveplates for the terahertz range

Surya Revanth Ayyagari, Andreas K Klein, Simonas Indrišiūnas, Vytautas Janonis, Daniil Pashnev, Abdu Subahan Mohammed, Guillaume Ducournau, Andreas Stöhr, Irmantas Kašalynas

► **To cite this version:**

Surya Revanth Ayyagari, Andreas K Klein, Simonas Indrišiūnas, Vytautas Janonis, Daniil Pashnev, et al.. Broadband high-contrast-grating-type waveplates for the terahertz range. Optics Express, 2024, Optics Express, 32 (9), pp.15870-15881. 10.1364/oe.521532 . hal-04569540

**HAL Id: hal-04569540**

**<https://hal.science/hal-04569540>**

Submitted on 6 May 2024

**HAL** is a multi-disciplinary open access archive for the deposit and dissemination of scientific research documents, whether they are published or not. The documents may come from teaching and research institutions in France or abroad, or from public or private research centers.








L'archive ouverte pluridisciplinaire **HAL**, est destinée au dépôt et à la diffusion de documents scientifiques de niveau recherche, publiés ou non, émanant des établissements d'enseignement et de recherche français ou étrangers, des laboratoires publics ou privés.



Distributed under a Creative Commons Attribution 4.0 International License



# Broadband high-contrast-grating-type waveplates for the terahertz range

SURYA REVANTH AYYAGARI,<sup>1,5</sup>  ANDREAS K. KLEIN,<sup>2</sup>  SIMONAS INDRIŠIŪNAS,<sup>3</sup>  VYTAUTAS JANONIS,<sup>1</sup>  DANIIL PASHNEV,<sup>1</sup> ABDU SUBAHAN MOHAMMED,<sup>4</sup> GUILLAUME DUCOURNAU,<sup>4</sup>  ANDREAS STÖHR,<sup>2</sup>  AND IRMANTAS KAŠALYNAS<sup>1,6</sup> 

<sup>1</sup>Terahertz Photonics Laboratory, Center for Physical Sciences and Technology (FTMC), Saulėtekio ave. 3, Vilnius LT-10257, Lithuania

<sup>2</sup>Department of Optoelectronics, University Duisburg-Essen, Forsthausweg 2, Duisburg 47057, Germany

<sup>3</sup>Laser Microfabrication Laboratory, Center for Physical Sciences and Technology (FTMC), Savanoriu ave. 231, Vilnius LT-02300, Lithuania

<sup>4</sup>Institut d'Electronique de Microélectronique et de Nanotechnologie (IEMN), Université de Lille, Villeneuve d'Ascq, Lille 59652, France

<sup>5</sup>surya.revanth@ftmc.lt

<sup>6</sup>irmantas.kasalynas@ftmc.lt

**Abstract:** The high-contrast-grating waveplates utilizing high contrast between silicon and air refractive indexes were developed in order to perform as a quarter wave and a half wave plate in the selected THz frequency range. The waveplates possessed anti-reflective properties due to the specific inclination of the walls both in parallel and in perpendicular direction to grating axis, efficiently suppressing the reflection losses caused by air-dielectric interface for both transverse magnetic and transverse electric polarizations. Moreover, significant reduction of the transmittance gap was achieved between both polarizations while mitigating overall Fabry-Perot effect. Validation of the concepts was carried out by measuring transmission amplitude and phase spectra of the fabricated samples in a broadband of THz time-domain spectroscopy and vector-network-analysis systems considering also some real applications.

Published by Optica Publishing Group under the terms of the [Creative Commons Attribution 4.0 License](https://creativecommons.org/licenses/by/4.0/). Further distribution of this work must maintain attribution to the author(s) and the published article's title, journal citation, and DOI.

## 1. Introduction

Terahertz (THz) radiation, occupying the electromagnetic (EM) spectrum range between micro- and infrared waves, ranging from 3 mm to 30  $\mu\text{m}$  wavelength (0.1 to 10 THz), has gained significant attention due to its unique properties and versatile applications across various domains. This region offers unique advantages, including the ability to penetrate non-conductive materials, non-ionizing nature, and low photon energy. These features make it suitable for a wide range of applications such as THz data communication [1], material spectroscopy [2], imaging [3], biomedical sensing [4] and scanning [5]. However, more efficient manipulation and control of EM wave phase and polarization, are essential for controlling the propagation of light and is a great necessity for the above-mentioned applications. Waveplates and phase retarders are essential components which manipulate and control the polarization state and phase of the EM wave. Usually, the waveplates are designed to introduce a defined phase delay between two orthogonal polarization components of EM wave.

Most commonly conventional methods for the control of phase and polarization depend on the intrinsic properties of natural birefringence materials, which support different phase delays along the two orthogonal optical axes. The number of easily applicable naturally birefringent materials is very limited in the THz range due to the small difference of the refractive indexes along optical

axes, large losses, bulk size, and high cost of material and production [6]. For example, natural birefringence in liquid crystals and crystalline quartz is low in the range of 0.3-0.5 THz is of 0.127 [7] and 0.046 [8], respectively. Therefore, due to their low birefringence the thickness of a waveplate can reach up to several millimeters and that makes them difficult to integrate with other THz devices. Moreover, low loss, THz transparent materials like silicon and polymers such as HDPE and Teflon are isotropic and possess no birefringence at all. Another of commonly used materials is lithium niobate (LiNbO<sub>3</sub>), with birefringence effect caused by its nonlinearity, but its use in THz range is hampered by high absorption losses [9].

Some of the ways to improve the operational bandwidth and to achieve a  $\pi$  phase retardation in the waveplate are the use of a multi-layer design taking advantage of natural material birefringence [10], or introduction of artificial birefringence via creation of some complex subwavelength structures [11,12], use of aperiodic gradient gratings [13] or Fresnel rhomb waveplate design [14].

Artificial birefringence has to be created either by producing periodic sub-wavelength structures or by surface modification introducing a spatial asymmetry which provides high order anisotropy [6,15]. One way to create an artificial birefringence is by creating a subwavelength grating on the surface [6] or in the volume of the material [16]. The surface structures are made by etching or ablating subwavelength periodic grooves with the periodicity of around  $\lambda/8$  and depth of  $\lambda/4$ . However, dielectric-grating-based waveplates seem to be more attractive than metal-based ones because of their low loss and phase retardation proportional to product of refractive index and physical thickness, called optical thickness at specific wavelength [9]. Though the dielectric-based grating waveplates are suitable for the manipulation of THz polarization in transmission mode because of high transparency, they still lack the operational bandwidth for broadband regime as the phase retardation is proportional to the frequency [13]. Moreover achieving a phase difference of  $\pi$  between the orthogonal polarization components is itself complicated for low refractive index materials [6].

Use of low-loss silicon as the waveplate material is advantageous because of its high thermal stability as compared to polymers as well as established processing techniques, especially when the device under test needs to undergo high-intensity laser fabrication and characterization methods [17]. Moreover, it stands out as one of the most transparent material with minimal absorption losses across the THz frequencies. Additionally, silicon exhibits low dispersion indicating that its refractive index remains constant regardless of the frequency in THz range. Important advantage for constructing a waveplate lies in its high refractive index with 3.45 as compared to polymer materials which are around 1.45 in THz frequencies. This characteristic enables silicon substrates to have a reduced physical thickness compared to polymers while still achieving the necessary phase retardation.

The high contrast grating (HCG) was proposed of a single layer of high-index-contrast sub-wavelength grating in which tailoring of the dispersion relations of two orthogonal waveguide-modes is supported by the structure [18,19]. As the periodic gratings merely resemble a periodic waveguide along the propagation direction a few waveguide modes are excited depending on the angle of incidence of the plane wave. Because of large index contrast and functional properties of HCG, only two waveguide modes with real propagation constants carries electromagnetic energy along the propagation direction for a wide frequency range. When the HCG subjected to normal incidence light only even modes are excited such as TE<sub>0</sub>/TM<sub>0</sub> and TE<sub>2</sub>/TM<sub>2</sub> whereas, under oblique incidence odd modes are excited. However, only zeroth order diffraction carries energy both in reflection and transmission because of HCG's subwavelength period in air [20].

In addition, there is some insertion loss for grating based waveplates due to strong reflection at the material-air interfaces which can be reduced by adding anti-reflection layers [21]. In the THz range, the broadband anti-reflective structures (ARS) of subwavelength dimensions were developed on crystalline material using mechanical dicing blade or direct laser ablation

techniques [22,23]. However, in micro structuring applications these techniques encounter certain limitations in terms of fabrication efficiency. Notably, issues such as surface roughness may arise, potentially causing scattering or diffraction losses, particularly at higher THz frequencies [17].

Thus, efficient manipulation and control of polarization of light requires a waveplate with wide operational bandwidth, achieving a phase difference of  $\pi/2$  or  $\pi$  between the orthogonal polarization components, and less reflection losses at high frequencies. To achieve all the above qualifications in a single component, the waveplate design becomes more complex and difficult to implement.

In this paper, we have designed and fabricated a monolayer HCG-type waveplate with an anti-reflective design which operates as quarter waveplate (QWP) in the frequency range of 0.3 to 0.5 THz providing operational bandwidth of 200 GHz. The waveplate consists of a periodic high resistivity floating zone silicon (HRFZ-Si)-air interface with a period of 100  $\mu\text{m}$  and grating height of 200  $\mu\text{m}$  and the inclination of walls on each side is 11 degrees on top surface of a HRFZ-Si wafer with overall thickness of 250  $\mu\text{m}$ . Such inclination of walls suppresses the Fabry-Perot effect in the TM polarization compared to the walls of grating with no inclination. In addition, to extend the performance of a QWP to half waveplate (HWP) and improve its transmission performance we have implemented such similar periodic dielectric-air interface gratings on both top and bottom sides of a HRFZ-Si silicon wafer. In this case overall wafer thickness was 500  $\mu\text{m}$  with a grating height of just 100  $\mu\text{m}$  on each side leaving a solid silicon material of 300  $\mu\text{m}$  in between. This structure possesses both QWP and HWP characteristics with improved transmission along TM polarization from 90% up to 100% in a broadband frequency range. To mitigate the overall Fabry-Perot effect in the TE polarization and narrow the transmission gap between TE and TM polarizations, we have implemented further modifications to the grating's surface along the TE-axis. We changed the surface design from a flat to a sinusoidal shape with the amplitude and period of 10  $\mu\text{m}$  and 1500  $\mu\text{m}$  respectively along TE polarization. As a result of these modifications, the overall Fabry-Perot effect has significantly diminished for both TE and TM polarizations and the transmission gap between both the polarizations has been successfully reduced to less than 10%, across a frequency range spanning from 0.3 to 0.9 THz.

## 2. Samples and methods

Monolayer HCG-type waveplates were developed of HRFZ-Si wafer employing the Direct Laser Ablation (DLA) technique [17]. In this context, the gratings are composed of periodic ridges of Si either on single or both sides of the wafer. The designed gratings on a HRFZ-Si induce controlled phase shifts between the orthogonal components of the incident THz wave due to the presence of artificial birefringence. The DLA was used for fabrication of surface gratings using a precisely focused laser beam to remove material from the substrate, enabling the creation of well-defined grooves and ridges. This technique offered exceptional control over the grating's shape and dimensions, ensuring a high level of precision and reproducibility. To assess the performance of the waveplates, the Finite Difference Time Domain (FDTD) simulations as well as the THz Time Domain spectroscopy (THz-TDS) and Vector Network Analyser (VNA) experiments were implemented investigating the transmission amplitude and phase spectra.

FDTD simulations were performed to optimize the waveplates transmission and phase spectra, using same solver as discussed in our previous works [23,24]. Simulations were carried out using a normal illumination of plane wave by choosing a perfectly matched layer boundary conditions to absorb the transmitted and reflected waves from the structure. The S-parameter calculations were performed for both TE and TM polarizations assuming the steady-state energy criterion using a multi-frequency plane wave incoming onto the sample.

The modelled waveplate with a periodic grating was patterned by an industrial-scale pulsed laser (Atlantic 60, EKSPLA UAB) with a operation wavelength of 1064 nm, 32  $\mu\text{m}$  laser spot size diameter, pulse duration of 10 ps, 11.8 J/cm<sup>2</sup> laser irradiation fluence, scan speed of 856

mm/s (47% spot overlap), hatch angle rotation of 45 degrees after each scan and etch depth of 0.2  $\mu\text{m}$  per layer which allowed to maintain precise control over the structure [17].

THz-TDS experiments were conducted to analyse the transmission spectra of the fabricated waveplate. The samples were characterized using a commercial THz-TDS system (TeraVil T-SPEC 800) in the frequency range of 0.1–2.0 THz at a room temperature. A significant advantage of THz-TDS is that the THz spectrum is complex-valued, meaning it provides amplitude and phase information at every frequency point. The transmission was defined as the squared ratio between the field amplitude of a waveplate and the field amplitude at the same point but without waveplate (air). The phase retardation ( $\Delta\varphi$ ) of a waveplate is calculated from the difference of phase from TE and TM orthogonal polarizations.

VNA measurements were carried out over a frequency range of 220 to 1100 GHz to study the transmission characteristics of a waveplate. Various wide range waveguides and frequency extenders were employed to achieve this frequency coverage. The VNA measurements were meticulously calibrated using a set of Thru/Reflect/Match (TRM) standards, following the TRM calibration procedure. Calibration was performed for WR3, WR2, WR1.5, and WR1 waveguide bands. S-parameters are used to describe the relationship between the input and output ports (or terminals) of the calibrated port of the VNA. For example, in a two-port setup comprising Port 1 and Port 2, S<sub>21</sub> represent the power transfer from Port 1 to Port 2. The incident beam from the WR waveguides were out-coupled to free-space using waveguide horn antennas, further manipulated through two parabolic mirrors before and after passing through the sample similar to the THz-TDs experiment. Additionally, absorbers were strategically employed within the WR waveguides to mitigate scattering effects.

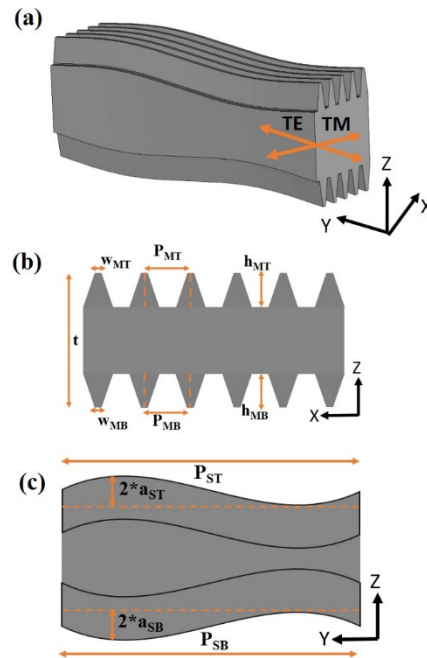
### 3. Results

Figure 1 shows the design of proposed HCG-type waveplate on dielectric wafer such as HRFZ-Si wafer. In the subsequent sections, we discuss the design and optimization details of a waveplate with experimental findings. Respective design parameters at the top and bottom of the waveplate, indicated in Fig. 1, can be different in general. However, in this paper we discuss cases where respective parameters on both sides of waveplate were kept equal.

#### 3.1. Design of flat profile single-sided HCG waveplate

Initially, single-sided monolayer HCG-type waveplate was developed with a subwavelength periodic material-air interfaces with a period of  $P_{\text{MT}} = 100 \mu\text{m}$  on top of a HRFZ-Si wafer with an overall thickness of  $t = 250 \mu\text{m}$ . The grating height of a waveplate was kept at  $h_{\text{MT}} = 200 \mu\text{m}$  i.e the height from the top of the ridge to the bottom of the groove. The width of the top of the ridges was kept at  $w_{\text{MT}} = 50 \mu\text{m}$ , resulting in sidewall inclination on each side of 11 degrees. It is worth to note that geometrical parameters were optimised numerically by performing numerous calculations with various parameter set and 3 selected cases were fabricated, results for best of which are reported in this paper. The sinusoid amplitude was kept at  $a_{\text{ST}} = 0 \mu\text{m}$  in this case maintaining the flat design in TE polarisation. We call the polarization along grating axis as transverse magnetic (TM) and perpendicular to the grating axis as transverse electric (TE) modes shown in Fig. 2(a). The required phase difference ( $\Delta\varphi$ ) between TE and TM orthogonal polarizations can be achieved by carefully choosing the proper height and width of a grating ridges. The grating profile and microscopic image of a fabricated waveplate is shown in Fig. 2(b) and 2(c).

The results of transmission and phase retardation ( $\Delta\varphi$ ) of a single-sided monolayer HCG-type waveplate for two orthogonal polarizations (TE and TM) are shown in Fig. 3. The transmission results for both the TE and TM polarizations were compared between the FDTD simulations, TDS and VNA measurements which shows a nice agreement in Fig. 3(a) and 3(b). In the TE polarization, the incoming light interacts only with the flat surfaces of the structure. Due to



**Fig. 1.** Proposed design of the monolayer HCG-type waveplate. (a) 3-D representation of a waveplate with periodic sinusoid patterning in TE polarization and meander patterning in TM polarization on both faces of the dielectric substrate, (b) shows the 2-D representation of a waveplate along XZ-axis (TM polarization). (c) shows the 2-D representation of a waveplate along YZ-axis (TE polarization). Annotations:  $P_{MT}$  and  $P_{MB}$  is the period of meander gratings;  $P_{ST}$  and  $P_{SB}$  – period of sinusoidal gratings;  $W_{MT}$  and  $W_{MB}$  – width of meander gratings;  $h_{MT}$  and  $h_{MB}$  – height of meander gratings;  $a_{ST}$  and  $a_{SB}$  – amplitude of sinusoidal modulation at the top and bottom surfaces, respectively;  $t$  - is the total thickness of waveplate.

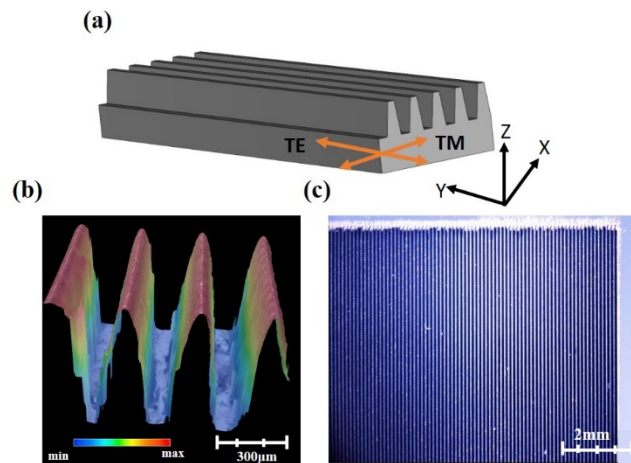


**Fig. 2.** The images of single-sided monolayer HCG-type waveplate; (a) 3D representation of a waveplate; (b) grating profile was shown in color scale along XZ-axis taken from the optical profilometer, showing grating ridges (red) and grating grooves (blue), (c) microscopic images of a waveplate along XY-axis.

strong internal reflection, standing waves form within the waveplate with corresponding well known Fabry-Perot periodic spectral characteristics [25]. The amplitude of such oscillations in transmission spectra for an un-patterned double-side polished Si wafer of 250  $\mu\text{m}$  thickness is around 70%, and for investigated structure in TE polarization it is around 50%. The Fabry-Perot effect for TM polarization is suppressed quite significantly (amplitude modulation of 10% in TM versus 50% in TE polarization) with the average transmission of silicon waveplate of about 70%. Figure 3(c) shows the phase retardation between TE and TM polarizations across the investigated frequency range. Region where the phase retardation of  $90 \pm 10$  degrees is achieved is marked by dashed lines. QWP operation is observed in the frequency range of 0.3 to 0.5 THz (bandwidth of 200 GHz). Inset shows the comparison of phase retardation results of a monolayer HCG-type waveplate with and without inclination of grating side walls considered by FDTD simulations. It is seen that Fabry-Perot effect is suppressed more with the inclination of side walls by 11 degrees, moreover, the phase keeps close to constant value of  $\pi/2$  and  $3\pi/4$  in broad frequency range at around frequencies of 400 GHz and 600 GHz, respectively.

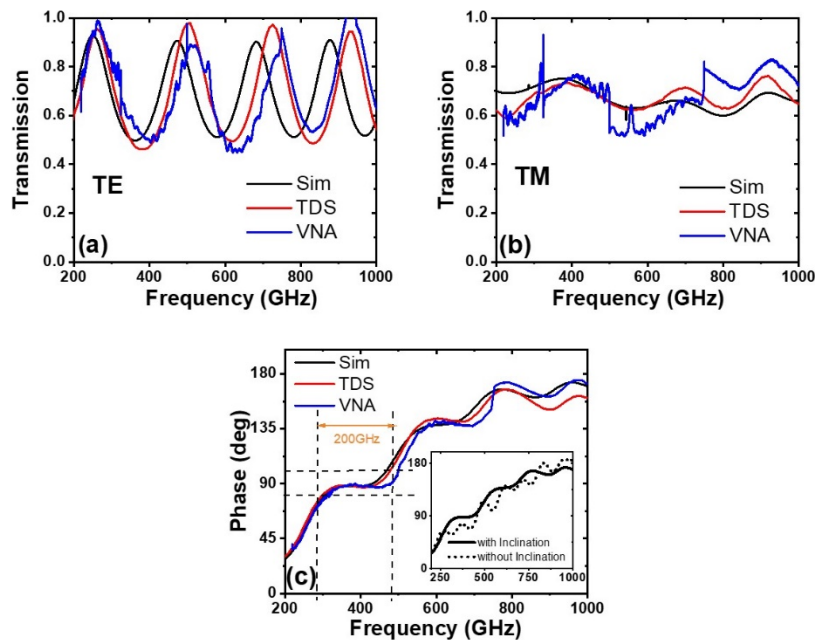


**Fig. 3.** Transmission and phase retardation characteristics of a single-sided monolayer HCG-type waveplate compared between FDTD simulations (black), THz-TDs setup (red) and VNA setup (blue), (a) along TE polarization (b) along TM polarization, and (c) phase difference between TE and TM polarizations. Inset: comparison of phase retardation of a waveplate with and without inclination of side walls. Note that the breaks in transmission for VNA are caused by the changing of WR ranges.

### 3.2. Design of flat profile double-sided HCG waveplate

To improve the transmission performance of a waveplate along the grating axis or TM polarization we've made a modification to the previously mentioned single-sided monolayer HCG-type waveplate changed it to double-sided monolayer HCG-type waveplate possessing anti-reflection properties, simultaneously reducing reflections within the structure as well as coupling losses between the component and free-space [23]. The double-sided grating waveplate consists of a similar subwavelength periodic material-air interfaces with a period of  $P_{\text{MT}} = P_{\text{MB}} = 100 \mu\text{m}$

on both top and bottom sides of a HRFZ-Si wafer with an overall thickness of  $t = 500 \mu\text{m}$ . The height of meander gratings on each side of a waveplate is exactly half of an initial grating height of a single sided sample with  $h_{\text{MT}} = h_{\text{MB}} = 100 \mu\text{m}$  leaving a solid layer of silicon in middle with a thickness of approximately  $300 \mu\text{m}$ . In Fig. 4. we observe a transmission spectrum along grating axis of a modified waveplate featuring a double-side grating which shows a remarkable enhancement of transmission approaching nearly to 100% for TM polarization. Additionally, it showcases a  $\pi$  phase shift between the two orthogonal polarizations which was not achieved in the previously mentioned single-sided waveplate. This enhanced transmission performance is observed within the frequency range of 0.434/0.369 THz to 0.979/0.860 THz with a broadband operational bandwidth of 545/491 GHz for the simulation/experimental findings respectively. Conversely, we can achieve the required  $\pi$  phase shift between TE and TM polarizations, enabling the waveplate to function as a HWP in the frequency range of 0.778 THz to 0.978 THz, with an operational bandwidth spanning 200 GHz in simulations. However, it is important to note that in our experimental findings, achieving such  $\pi$  phase shift has proven challenging due to fabrication errors. We see in the experimental results that to achieve  $\pi$  phase shift as obtained in simulations additional refining of the DLA technology for processing of double-sided samples is required. Simultaneously, at lower frequencies ranging from 0.327/0.300 THz to 0.403/0.382 THz, a  $\pi/2$  phase shift is achieved with bandwidth of 76/82 GHz for simulations/experimental findings, offering a dual-band waveplate performance for a broadband spectrum of THz frequencies.

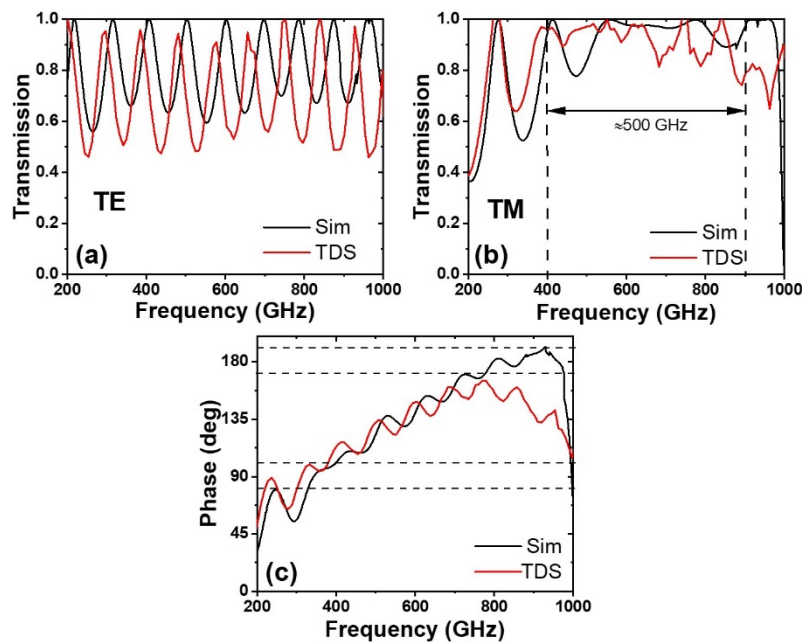


**Fig. 4.** Characterization results of double-sided monolayer HCG-type waveplate compared with FDTD simulation (black) and THz-TDS setup (red): transmission spectra for (a) TE polarization and (b) TM polarization and (c) phase difference.

### 3.3. Design of sinusoidal profile HCG waveplate

In order to mitigate the Fabry-Perot effect along the TE polarization and with an aim to maintain smooth overall transmission of a waveplate across the frequency range we have introduced a surface modification along TE-axis of the waveplate. In other words, to reduce the instability of transmission caused by the multiple Fabry-Perot peaks and dips, the flat shape of the grating



was changed to a sinusoidal grating along TE polarization as shown in Fig. 5(a). In Fig. 5(b) the sinusoidal profile of a fabricated sample is shown in a color scale with ridges represented in red and grooves in blue colors. The sinusoidal single-sided grating waveplate consists of a similar subwavelength periodic material-air interfaces with a period of  $P_{MT} = 100 \mu\text{m}$  on top of a HRFZ-Si wafer with an overall thickness of  $t = 250 \mu\text{m}$ . The grating height of a waveplate was kept at  $h_{MT} = 200 \mu\text{m}$  and the amplitude  $a_{ST} = 25 \mu\text{m}$  transitioning flat shape to sinusoidal shape along TE polarization with a sinusoidal period of  $P_{ST} = 1500 \mu\text{m}$ . The results of transmission of a sinusoidal grating waveplate for two orthogonal polarizations (TE and TM) are shown in Fig. 5(c) and 5(d).

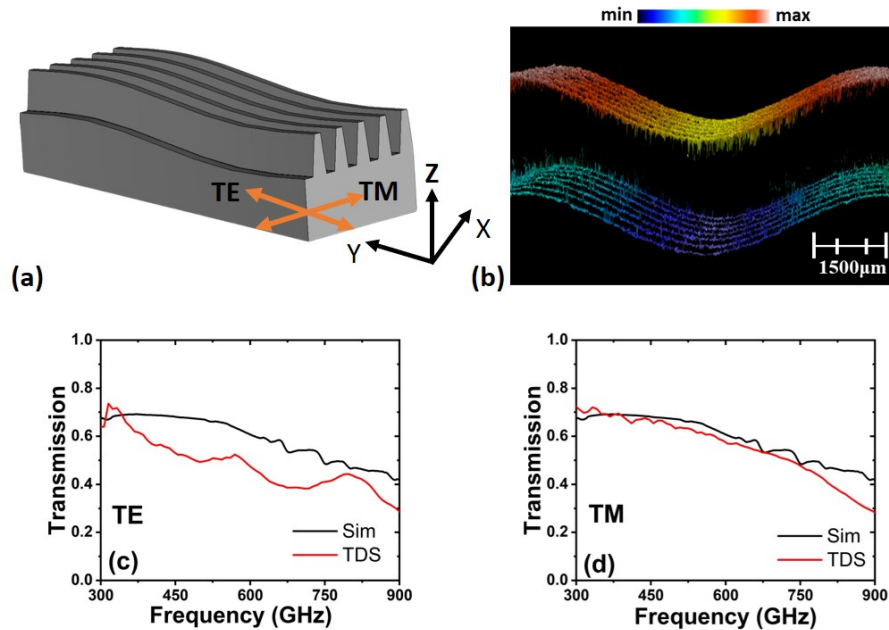


**Fig. 5.** (a) 3D representation of a sinusoidal shape single-sided monolayer HCG-type waveplate (b) representing a sinusoidal grating profile shown in color scale along YZ-axis with a sinusoidal modification along TE axis taken from the optical profilometer, showing grating ridges (red) and grating grooves (blue). (c) and (d) Transmission spectra of sinusoidal single-sided monolayer HCG with the FDTD simulation (black) and THz-TDS setup (red): for TE and TM polarizations respectively.

In Fig. 5(c), we clearly observe a reduction of Fabry-Perot effect along TE polarization when compared to the above-mentioned flat design. Additionally, the transmission gap between TE and TM polarizations has been effectively minimized to below 10%. However, there is a significant decrease in transmission for both polarizations at higher frequencies. Given that the waveplate's intended function is in transmission mode, the observed low transmission is undesirable.

To improve the transmission performance of a waveplate at higher frequencies and narrow the transmission gap between TE and TM polarizations, we have implemented further adjustments to the sinusoidal single-sided HCG. This modification transforms the sinusoidal single-sided grating to sinusoidal double-sided grating, featuring a sinusoidal modulation on both top and bottom side of a HRFZ-Si with an amplitude of  $a_{ST} = a_{SB} = 10 \mu\text{m}$  and a modulation period of  $P_{ST} = P_{SB} = 1500 \mu\text{m}$ , as depicted in Fig. 1(c). As a result of these modification, the transmission of a waveplate improves significantly at higher frequencies. Simultaneously, the successful reduction of the transmission gap between TE and TM polarizations to less than 10% is achieved, all while ensuring that the overall Fabry-Perot effect remains diminished. Moreover, now the

overall transmission of the waveplate exceeds 60% within the frequency range around 0.3 to 0.9 THz as it is shown in Figs. 6(a) and 6(b). Furthermore, this modified waveplate still works as a QWP for a frequency of 0.300 to 0.391 THz offering an operational bandwidth of 91 GHz and operates as HWP for a frequency range of 0.713 to 0.924 THz providing an operational bandwidth of 211 GHz still showing dual-band waveplate performance for a broadband THz frequency range (see Fig. 6(c)).

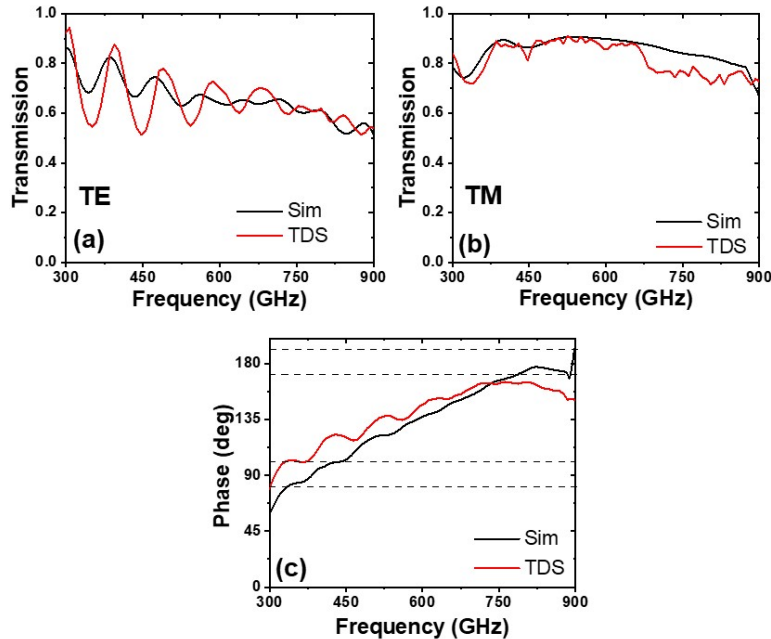


**Fig. 6.** Transmission results of the sinusoidal double-sided monolayer HCG compared with FDTD simulation (black) and THz-TDS setup (red): transmission spectra for (a) TE polarization, (b) TM polarization and (c) phase difference.

### 3.4. Polarization control with the QWP sample

We conducted experimental research to demonstrate real application of the single-sided monolayer HCG waveplate with a commercial THz frequency domain system by utilizing Toptica Terascan 780 spectrometer setup. The results are shown in the Fig. 7. To determine the sample's suitability as a QWP within a specified frequency bandwidth (0.3 to 0.5 THz), experiments were carried out at an intermediate frequency of 0.4 THz. Initially, we established a straightforward configuration in which linearly polarized light along the TE and TM axes was entirely blocked, but allowing circularly polarized light to be detected if QWP is inserted in between the elements at the angle of  $45^\circ$ . This setup comprised of a THz emitter emitting circular polarized THz radiation, a  $0^\circ$  polarizer converting circular to linear polarization (either vertical or horizontal), an analyzer oriented perpendicularly ( $90^\circ$ ) to the polarizer to block linearly polarized light, and a THz detector. Subsequently, the sample was introduced into the optical path at a  $45^\circ$  angle relative to both the polarizer and analyzer (blue color line). Remarkably, we observe increase of the signal transmission as detected by the THz detector in the spectrum range of 300-500 GHz, confirming that the designed sample performs as a QWP.

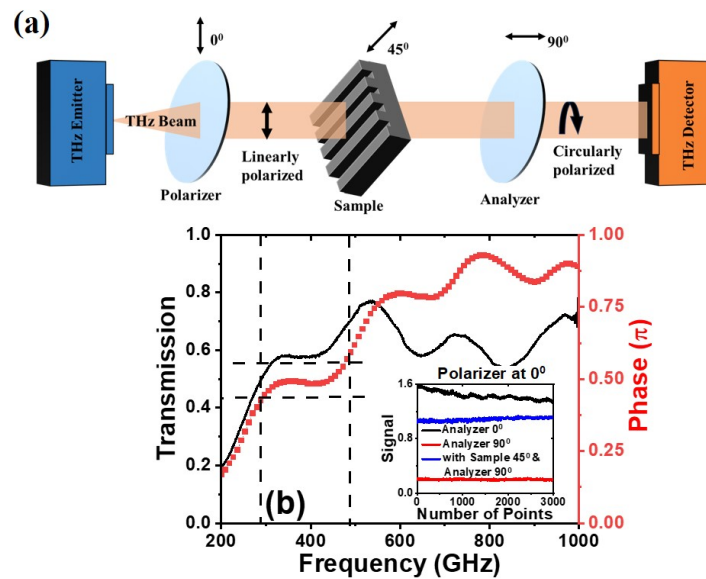


**Fig. 7.** (a) Schematic representation of polarization measurement setup, (b) absolute transmission (left) of a waveplate measured exactly with the above shown setup configuration and the phase characteristics (right) of a waveplate normalized to  $\pi$  across the frequencies up to 1 THz. Inset: signal measurements in transmission mode at fixed 400 GHz frequency with both polarizer and analyzer placed parallel (black curve); with both crossed (red curve) and with the sample placed in between and oriented at 45 degrees (blue curve).

#### 4. Conclusions

In conclusion, broadband, artificially birefringent High-Contrast-Grating-type waveplates were designed and fabricated for THz frequency range. The developed single-sided monolayer HCG operating as a quarter waveplate (QWP) in the frequency range of 0.3 to 0.5 THz, with a broadband operational bandwidth of 200 GHz is presented both theoretically and experimentally. The proposed waveplates exhibits anti-reflective behavior along TM polarization due to inclination of grating walls effectively suppressing the reflection losses caused by silicon-air interface. The single-sided monolayer HCG-type waveplate performs admirably as a QWP, however it encounters difficulties in achieving a 180-degree or  $\pi$  phase shift to work as a HWP. To address this challenge and simultaneously mitigate reflection losses with enhancing the transmission of the waveplate, we have implemented similar grating structure on the opposite side of the sample. By incorporating of such grating structures on the top and bottom side of the sample we enhance the transmission performance of the waveplate reaching up to 100% with an overall bandwidth of 500 GHz. In addition, by changing the shape of grating along the TE-axis from a flat to sinusoidal shape with specific amplitude and period, the overall Fabry-Perot effect within the HRFZ-Si material is mitigated. This transition also significantly reduces the transmission gap between TE and TM polarizations, thereby enhancing the device's performance. Operation at other frequencies can be achieved by scaling the geometrical parameters of the structures. Therefore, such waveplates with high transmission and phase retardation holds immense promise for applications requiring precise polarization control and efficient terahertz wave transmission. Overall, this research marks a significant step forward in the development of advanced waveplate technologies, offering a path toward more efficient and versatile terahertz devices in the control of phase and polarization of THz wave.

**Funding.** H2020 Marie Skłodowska-Curie Actions (956857); Lietuvos Mokslo Taryba (DOTSUT-184); Agence Nationale de la Recherche (ANR-22-PEEL-0006, ANR-22-PEFT-0006, ANR-21-ESRE-0007).

**Acknowledgments.** This work received funding through the EU TERAOPTICS project (grant no. 956857) under the program H2020-EU.1.3.1. topic MSCA-ITN-2020 and through the “Hybrid plasmonic components for THz range (T-HP)” project (grant no. DOTSUT-184) of the Research Council of Lithuania (Lietuvos Mokslo Taryba) funded by the European Regional Development Fund according to the Measure No. 01.2.2-LMT-K-718-03-0096.

VNA measurements supported by the France 2030 programs, PEPR (Programmes et Equipements Prioritaires pour la Recherche), CPER Wavetech, University of Lille, and Ultra-High Data-rate (UHD) IEMN flagship. The PEPR is operated by the Agence Nationale de la Recherche (ANR), under the grants ANR-22-PEEL-0006 (FUNTERA) and ANR-22-PEFT-0006 (NF-SYSTERA). The Contrat de Plan Etat-Region (CPER) WaveTech is supported by the Ministry of Higher Education and Research, the Hauts-de-France Regional Council, the Lille European Metropolis (MEL), the Institute of Physics of the French National Centre for Scientific Research (CNRS) and the European Regional Development Fund (ERDF). The work was also supported by the ADD4P project, operated by ANR (Grant 21-ESRE-0007) for the experimental characterization steps carried out at the CNRS-IEMN.

**Disclosures.** The authors declare no conflicts of interest.

**Data availability.** Data underlying the results presented in this paper are available upon reasonable request.

## References

1. T. Nagatsuma, G. Ducournau, and C. C. Renaud, “Advances in terahertz communications accelerated by photonics,” *Nat. Photonics* **10**(6), 371–379 (2016).
2. P. U. Jepsen, D. G. Cooke, and M. Koch, “Terahertz spectroscopy and imaging - Modern techniques and applications,” *Laser Photonics Rev.* **5**(1), 124–166 (2011).
3. S. Watanabe, “Terahertz polarization imaging and its applications,” *Photonics* **5**(4), 58 (2018).
4. H. Yoshida, Y. Ogawa, Y. Kawai, *et al.*, “Terahertz sensing method for protein detection using a thin metallic mesh,” *Appl. Phys. Lett.* **91**(25), 25–28 (2007).
5. T. L. Cocker, V. Jelic, M. Gupta, *et al.*, “An ultrafast terahertz scanning tunnelling microscope,” *Nat. Photonics* **7**(8), 620–625 (2013).
6. M. Chen, F. Fan, S. T. Xu, *et al.*, “Artificial high birefringence in all-dielectric gradient grating for broadband terahertz waves,” *Sci. Rep.* **6**(1), 38562–11 (2016).
7. C.-S. Yang, C.-J. Lin, R.-P. Pan, *et al.*, “The complex refractive indices of the liquid crystal mixture E7 in the terahertz frequency range,” *J. Opt. Soc. Am. B* **27**(9), 1866 (2010).
8. D. Grischkowsky, S. Keiding, M. van Exter, *et al.*, “Far-infrared time-domain spectroscopy with terahertz beams of dielectrics and semiconductors,” *J. Opt. Soc. Am. B* **7**(10), 2006 (1990).
9. Y. Gong, Z. Zhang, J. Tang, *et al.*, “Research progress on terahertz achromatic broadband polarization wave plates,” *Opt. Laser Technol.* **166**(March), 109633 (2023).
10. Z. Chen, Y. Gong, H. Dong, *et al.*, “Terahertz achromatic quarter wave plate: Design, fabrication, and characterization,” *Opt. Commun.* **311**, 1–5 (2013).
11. A. Moreno-Peñarrubia, S. A. Kuznetsov, and M. Beruete, “Ultrathin subterahertz half-wave plate with high conversion efficiency based on zigzag metasurface,” *IEEE Trans. Antennas Propagat.* **68**(11), 7700–7704 (2020).
12. Y. Nakata, Y. Taira, T. Nakanishi, *et al.*, “Freestanding transparent terahertz half-wave plate using subwavelength cut-wire pairs,” *Opt. Express* **25**(3), 2107 (2017).
13. Y. Yuan, J. Cheng, X. Dong, *et al.*, “Terahertz dual-band polarization control and wavefront shaping over freestanding dielectric binary gratings with high efficiency,” *Opt. Lasers Eng.* **143**(April), 106636 (2021).
14. S. Mou, A. D’Arco, L. Tomarchio, *et al.*, “Achromatic terahertz quarter-wave Fresnel rhomb retarder,” *Appl. Phys. Lett.* **122**(24), 241102 (2023).
15. B. Päivänranta, N. Passilly, J. Pietarinen, *et al.*, “Low-cost fabrication of form-birefringent quarter-wave plates,” *Opt. Express* **16**(21), 16334 (2008).
16. Y. Shimotsu, P. G. Kazansky, J. Qiu, *et al.*, “Self-Organized Nanogratings in Glass Irradiated by Ultrashort Light Pulses,” *Phys. Rev. Lett.* **91**(24), 247405 (2003).
17. S. Indrišiusas, E. Svirplys, H. Richter, *et al.*, “Laser-Ablated Silicon in the Frequency Range From 0.1 to 4.7 THz,” *IEEE Trans. THz Sci. Technol.* **9**(6), 581–586 (2019).
18. W. Liu, T. Yu, Y. Sun, *et al.*, “Highly Efficient Broadband Wave Plates Using Dispersion-Engineered High-Index-Contrast Subwavelength Gratings,” *Phys. Rev. Applied* **11**(6), 064005 (2019).
19. V. Karagodsky and C. J. Chang-Hasnain, “Physics of near-wavelength high contrast gratings,” *Opt. Express* **20**(10), 10888 (2012).
20. C. J. Chang-Hasnain and W. Yang, “High-contrast gratings for integrated optoelectronics,” *Adv. Opt. Photon.* **4**(3), 379 (2012).
21. J. Zi, Q. Xu, Q. Wang, *et al.*, “Antireflection-assisted all-dielectric terahertz metamaterial polarization converter,” *Appl. Phys. Lett.* **113**(10), 101104 (2018).
22. T. Nitta, Y. Sekimoto, K. Noda, *et al.*, “Broadband Pillar-Type Antireflective Subwavelength Structures for Silicon and Alumina,” *IEEE Trans. THz Sci. Technol.* **7**(3), 295–301 (2017).

23. M. Tamosiunaite, S. Indrišūnas, V. Tamosiūnas, *et al.*, “Focusing of Terahertz Radiation With Laser-Ablated Antireflective Structures,” *IEEE Trans. THz Sci. Technol.* **8**(5), 541–548 (2018).
24. S. R. Ayyagari, S. Indrišūnas, and I. Kašalynas, “Hybrid Multiphase Fresnel Lenses on Silicon Wafers for Terahertz Frequencies,” *IEEE Trans. THz Sci. Technol.* **13**(3), 231–236 (2023).
25. W. Withayachumnankul and M. Naftaly, “Fundamentals of Measurement in Terahertz Time-Domain Spectroscopy,” *J. Infrared, Millimeter, Terahertz Waves* **35**(8), 610–637 (2014).